The electronic properties of an oxygen vacancy at ZrO_2-terminated (001) surfaces of a cubic $PbZrO_3$: computer simulations from the first principles

E. A. Kotomin,[ab] S. Piskunov,*[ac] Yu. F. Zhukovskii,[a] R. I. Eglitis,[ad] A. Gopejenko[a] and D. E. Ellis[e]

Received 18th February 2008, Accepted 29th April 2008
First published as an Advance Article on the web 11th June 2008
DOI: 10.1039/b802740d

Combining B3PW hybrid exchange–correlation functional within the density functional theory (DFT) and a supercell model, we calculated from the first principles the electronic structure of both ideal $PbZrO_3$ (001) surface (with ZrO_2- and PbO-terminations) and a neutral oxygen vacancy also called the *F* center. The atomic relaxation and electronic density redistributions are discussed. Thermodynamic analysis of pure surfaces indicates that ZrO_2 termination is energetically more favorable than PbO-termination. The O vacancy on the ZrO_2-surface attracts $\approx$0.3 e (0.7 e in the bulk $PbZrO_3$), while the remaining electron density from the missing O^{2-} ion is localized mostly on atoms nearest to a vacancy. The calculated defect formation energy is smaller than in the bulk which should lead to the vacancy segregation to the surface. Unlike Ti-based perovskites, the vacancy-induced (deep) energy level lies in $PbZrO_3$ in the middle of the band gap.

I. Introduction

Lead zirconate, $PbZrO_3$ (hereafter PZ), due to its antiferroelectric (AFE) behavior has many technologically important applications including actuators, capacitors and charge storage devices.[1–4] Thus, it is not surprising that in recent years PZ has been the subject of many experimental and theoretical studies.[1–13] The orthorhombic AFE phase is stable below 520 K, above this temperature PZ possesses a cubic structure with the lattice constant of 4.161 Å.[12] The PZ band gap is 3.7 eV. A field-induced ferroelectric phase transition is found feasible in PZ thin films due to a small free energy difference between the ferroelectric (FE) (rhombohedral) and the AFE phases.[12,13] Recently, AFE PZ thin film heterostructures have been found to be radiation resistant and were suggested as a promising candidate for application in radiation environments, including diagnostic materials and bolometers for thermonuclear reactors.[14] PZ serves also as a parent compound for $PbZr_{1-x}Ti_xO_3$ (PZT) solid solutions which are of high scientific and technological interest due to their ferroelectricity and piezoelectricity observed over a wide range of compositions.

The ABO_3-type perovskite crystals have been extensively studied because of their technological potential and because of fundamental interest in the physics of phase transition. They belong to a class of the most important ferroelectric materials. The perfect (cubic) perovskite structure is the simple $Pm\bar{3}m$ space group and has a full cubic symmetry, in which the body-center position is occupied by B atoms, the corners by A atoms and the face centers by oxygen atoms. The main defect in perovskite structure is O vacancy, also called the *F* center. The properties of the *F* center in perovskite bulk were summarized recently in a review article.[15] Surface defects considerably affecting the properties of thin perovskite films are practically not studied.

It is well known that the Hartree–Fock (HF) method considerably overestimates the optical gap of wide-gap materials, while local density approximation (LDA), as well as generalized gradient approximation (GGA) within DFT considerably underestimate it. The hybrid exchange–correlation functionals, B3PW and B3LYP, allow us to achieve the best possible agreement with experiment for the band gap calculated, *e.g.*, for $SrTiO_3$, $BaTiO_3$, and $PbTiO_3$ bulk perovskites, as it was shown in our previous studies.[16–18] Encouraged by the excellent agreement of the calculated band gap with experimental data for the three above mentioned perovskites, which is especially important for the defect studies, and our recent study of the PZ bulk in both cubic and AFE phases,[19] in the present paper we applied the hybrid B3PW method for the analysis of the PZ surface atomic/electronic structure and the *F* center on PZ surface.

II. Computational details

To perform the first-principles DFT-B3PW calculations, we have used the CRYSTAL-06 computer code.[20] In the B3PW functional the HF nonlocal exchange is mixed with the local

[a] *Institute of Solid State Physics, University of Latvia, 8 Kengaraga Street, Riga, LV-1063, Latvia*
[b] *Max-Planck-Institute for Solid State Research, Heisenbergstr., 1, D-70569 Stuttgart, Germany*
[c] *Theoretical Chemistry Department, University Duisburg-Essen, Universitätstr. 2, 45141 Essen, Germany. E-mail: sergej.piskunov@uni-due.de*
[d] *Department of Physics and Astronomy, Rutgers University, Piscataway, New Jersey 08855-0849, USA*
[e] *Department of Physics and Astronomy, Northwestern University, Evanston, Illinois 60208-3108, USA*

DFT exchange, using Becke three-parameter method,[21] combined with the non-local correlation functionals by Perdew and Wang.[22–24] The CRYSTAL code employs Gaussian-type functions (GTF) localized at atoms as the basis for expansion of the crystalline orbitals. In order to employ the LCAO-GTF (linear combination of atomic orbitals) method, it is desirable to optimize the localized basis sets (BS). Such optimization for a range of ABO_3 perovskites was developed and discussed by us.[16,17] In the present paper, the BSs for lead and oxygen have been taken from ref. 16: (O)—8-411(1d)G, (Pb)—211(1d)G, while the BS 311(31d)G (Zr) has been adopted from the CRYSTAL website.[20] The inner core electrons of Pb and Zr atoms were described by Hay-Wadt effective core pseudopotentials, taking into account the relativistic effect.[25,26] Besides a reasonable lattice constant,[16] our BSs for Pb and O also allowed us to achieve the excellent results for $PbTiO_3$ (001) surface relaxation and the surface band structure.[17] The reciprocal space integration was performed by sampling the Brillouin zone of the unit cell with the $8 \times 8 \times 8$ Pack-Monkhorst net.[27]

Another advantage of the CRYSTAL code is its treatment of purely 2-D slabs, without artificial periodicity in the direction perpendicular to the surface, unavoidably used in plane-wave surface calculations (*e.g.* ref. 28 and 29). In our calculations for the PZ (001) pure cubic surfaces, we have used a 2-D 11-layer slab model described elsewhere.[18] All atoms in a slab unit cell were allowed to relax (using a modified conjugate gradient algorithm[30,31]), in order to locate a minimum on the potential-energy surface (PES). We are familiar with the only first-principles DFT plane-wave calculations for pure PZ surfaces using smaller 7-plane slabs[32] which is discussed below.

To simulate the surface *F* center on ZrO_2 terminated PZ (001) surface, we have used a $2\sqrt{2} \times 2\sqrt{2}$ and 3×3 surface supercells with one of the surface O atoms removed (surface defect concentrations are 1/16 and 1/18, respectively). For an accurate description of the *F* center, an additional basis function has been placed into the oxygen vacancy, corresponding to the so-called *ghost* atom.[20] For this, we have used the same GTF as that used for the O^{2-} ions of the bulk PZ.

III. Results and discussions

A Ideal surfaces

Properties of a pure PZ bulk and the *F* centers therein were discussed by us recently.[19] The effective (Mulliken) atomic charges are given in the heading of Table 1, the calculated band gap (3.8 eV) is in perfect agreement with the experimental value (3.7 eV).

We performed here *ab initio* calculations of pure PbO- and ZrO_2-terminated (001) surfaces. The calculated (001) surface energy (0.95 eV/a_0^2) is close to that for $SrTiO_3$, $BaTiO_3$ and $PbTiO_3$ (001) surfaces[17,33] and 1.12 eV/a_0^2 found in DFT-PW PZ (001) calculations.[32]

Tables 1 and 2 show the electronic charge redistribution for the two terminations with respect to the bulk (Mulliken) charges (indicated in the heading of the former). The Pb effective charges on the PbO-terminated surface layer are smaller than in the bulk, as well as O charges. In contrast, the Zr charges on the ZrO_2-terminated surface are slightly increased. The charges in the deeper slab layers are very close to the relevant Pb, Zr, and O charges in the bulk.

Table 1 The results for PbO-terminated $PbZrO_3$(001) and 11-plane slab unit cell. The calculated atomic displacements along the *z*-axis in surface layers, d_z (in percentage of the equilibrium cubic lattice constant a_0 = 4.177 Å), with respect to atomic positions in bulk, changes of the effective Mulliken atomic charges, ΔQ (in e), with respect to the $PbZrO_3$ bulk (Pb 1.30 e, Zr 2.07 e, O −1.12 e), optical band gap, $\Delta\varepsilon_{gap}$ (in eV), and surface rumpling *s* (per cent a_0). Negative sign means displacement towards the slab center. The numbers in brackets are results of the CASTEP DFT-PW 7-plane calculations[32]

Layer	Atom	d_z	ΔQ
I	Pb	−6.95(−4.9)	−0.034(−0.65)
	O	−0.04(1.2)	−0.020(0.05)
II	Zr	2.57(2.6)	0.033(0.26)
	O	1.08(0.9)	−0.030 0.04)
III	Pb	−2.63(−1.1)	0.007(−0.29)
	O	−0.26(0.3)	−0.014(0.04)
IV	Zr	0.58	0.001
	O	0.15	−0.011
V	Pb	−0.62	0.007
	O	−0.08	−0.006
VI	Zr	0.00	0.000
	O	0.00	−0.001
s		6.91(6.1)	
$\Delta\varepsilon_{gap}$		3.13(1.8)	

This moderate charge redistribution is in contrast to the DFT-PW calculations[32] which suggest a basically similar trend but differs in the orders of magnitude. We attribute this to the use of the Mulliken population analysis for PW calculated electron density. This results in nonrealistic charges of atoms in pure PZ: Pb (1.6 e), Zr(0.98 e), and O (−0.86 e).

The difference electron density maps, calculated with respect to Pb^{2+}, Zr^{4+}, and O^{2-} ions, plotted in Fig. 1a and b, demonstrate a considerable covalency contribution in the Zr–O chemical bonds and a weak covalent bonding between Pb and O atoms. The Pb atoms nearest to the surface are polarized. Their electronic density is shifted outwards on the PbO-terminated surface. For the ZrO_2 terminated PZ (001) surface, the Zr–O bond nearest to the surface becomes stronger, but the next nearest bond becomes weaker as compared to $PbZrO_3$ bulk.

Calculated bond populations between atoms on the PZ (001) surface show that the major effect observed here is

Table 2 The same as in Table 1 for ZrO_2-terminated $PbZrO_3$(001)

Layer	Atom	d_z	ΔQ
I	Zr	−2.97(−1.9)	0.063(0.3)
	O	−1.36(−0.5)	−0.015(0.06)
II	Pb	5.54(4.7)	−0.013(−0.4)
	O	0.84(1.1)	0.036(0.1)
III	Zr	−1.12(−0.3)	0.001(0.16)
	O	−0.53(0.3)	0.004(0.06)
IV	Pb	1.39	0.002
	O	0.14	−0.003
V	Zr	−0.27	0.001
	O	−0.12	−0.002
VI	Pb	0.00	0.004
	O	0.00	−0.005
s		1.61(1.4)	
$\Delta\varepsilon_{gap}$		4.00(unknown)	

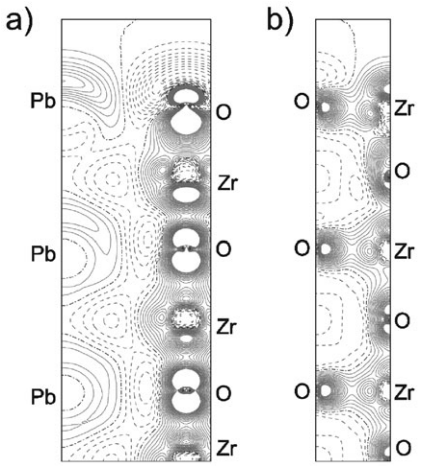

Fig. 1 Difference electron charge density maps (with respect to the superposition of densities of Pb^{2+}, Zr^{4+}, and O^{2-} ions) in the cross-sections perpendicular to the (110) surface with PbO termination (a) and in the cross-sections perpendicular to the (100) surface with ZrO_2 terminations (b). Full, dashed and dot-dashed lines denote the electron excess, deficiency, and zero-charge lines, respectively. The increment is 0.015 e a.u.$^{-3}$.

strengthening of the Zr–O and Pb–O chemical bonds near the ZrO_2- and PbO-terminated surfaces. The bond population between Zr and O atoms in the upper layer of the ZrO_2 terminated surface (236 me) more than twice exceeds the same in the bulk (100 me). The bond population between Pb and O atoms in the upper layer of PbO terminated surface also considerably (54 me or 50%) exceeds that in the bulk (36 me). At deeper layers of the PZ (001) surfaces, the bond populations between Zr and O, as well as Pb and O atoms are practically the same as in bulk. The similar effect of a strengthening of the Ti–O chemical bond was observed earlier by us for the $SrTiO_3$, $BaTiO_3$, and $PbTiO_3$ (001) surfaces.[17]

The calculated atomic displacements for the two terminations are given in Tables 1 and 2. In both cases the O atom goes above the Pb(Zr) atom which leads to surface *rumpling*. Its magnitude s is much larger for the PbO termination than for the ZrO_2. This is well reproduced in the DFT-PW calculations.[32] Atomic displacements are decreasing at deeper planes but are still considerable in the 5th plane from the surface.

The band gap of the pure PbO-terminated surface is considerably reduced (by 0.66 eV, Table 3). On the ZrO_2 termination, it is slightly increased, probably due to increased Zr effective charge on the surface. In the case of $SrTiO_3$ we have observed gap reduction for both terminations, SrO and TiO_2.[33] It should be noted here that the calculated band gaps depend also on the size of the supercell used: larger cells permit more complicated surface reconstructions from cubic towards the orthorhombic structure which leads to a slight increase of the band gap (Table 3, rows 3 and 4). This increase does not depend on the choice of the k-set used.

The calculated total and projected density of states (DOS) for both terminations (Fig. 2) shows that O 2p orbitals form the top of valence band, while the conduction band bottom consist of a mixture of Zr 4d and Pb 6s and 6p orbitals.

B Thermodynamics

The thermodynamic formalism adopted in the present study to estimate the stability of both PbO- and ZrO_2-terminated PZ (001) surfaces in equilibrium with matter reservoirs has been comprehensively described in ref. 34 (see also references therein). The analysis presented here assumes that all species are in thermodynamic equilibrium with all reservoirs, including oxygen atmosphere. The most stable surface is the one which minimizes the Gibbs free surface energy within the range of allowed values for Pb, Zr, and O chemical potentials:

$$\begin{aligned}\Omega(T,p) = \frac{1}{2A}[&G^{\text{slab}} - N_{\text{Ti}}\gamma^{\text{bulk}}_{\text{PbZrO}_3}(T,p) \\ &- (N_{\text{Pb}} - N_{\text{Zr}})\mu_{\text{Pb}}(T,p) \\ &- (N_{\text{O}} - 3N_{\text{Zr}})\mu_{\text{O}}(T,p)],\end{aligned} \tag{3.1}$$

where G^{slab} is the Gibbs free energy of the slab, which depends on the temperature, oxygen pressure, and on the number of atoms in the considered reservoirs N_i (i = Pb, Zr, and O), μ_i the chemical potentials of each species involved, and $\Omega(T, p)$ energy per unit of surface area A. The factor $\frac{1}{2}$ appears since a surface system is modeled by a slab with two equivalent surfaces. In eqn (3.1) we assume that the macroscopic quantities of PZ bulk material are in equilibrium with surface and O_2 environment. Thus, the chemical potentials are mutually dependent through the Gibbs free energy of the bulk perovskite:

$$\mu_{\text{Pb}}(T,p) + \mu_{\text{Zr}}(T,p) + 3\mu_{\text{O}}(T,p) = \gamma_{\text{PbZrO}_3}{}^{\text{bulk}}(T,p), \tag{3.2}$$

where γ hereafter denotes the Gibbs free energy per formula unit in a crystal. The Gibbs free energies of PZ bulk and slab can be estimated from first-principles calculations, evaluating their total energies. The vibrational contributions to the surface Gibbs free energies are small and can be neglected in comparison with errors in electronic structure computations.[34] Therefore, it is possible to replace the slab and the bulk Gibbs free energies by the corresponding total energies.

Table 3 Perfect and defective bulk and ZrO_2-terminated (001) surfaces of a cubic $PbZrO_3$. Optical band gap, $\Delta\varepsilon_{\text{gap}}$ (in eV), position of defective level with respect to the bottom of conduction band, $\Delta\varepsilon^F_{CB}$ (in eV), dispersion of a defect level, δ (in eV), effective Mulliken charge, ΔQ^F (in e), induced in the vacancy, and the energy of defect formation, E^F_{form} (in eV) as calculated by means of the B3PW hybrid exchange–correlation functional within DFT and 7-plane slab supercells

	$\Delta\varepsilon_{\text{gap}}$	$\Delta\varepsilon^F_{CB}$	δ	ΔQ^F	E^F_{form}
Perfect bulk	3.79	—	—	—	—
Bulk F-center	3.97	1.72	0.14	−0.68	7.25
SC $2\sqrt{2} \times 2\sqrt{2}$	4.47	—	—	—	—
SC 3×3	4.68	—	—	—	—
F-center, SC $2\sqrt{2} \times 2\sqrt{2}$	4.65	2.44	0.06	−0.30	5.82
F-center, SC 3×3	4.73	2.58	0.03	−0.31	7.00

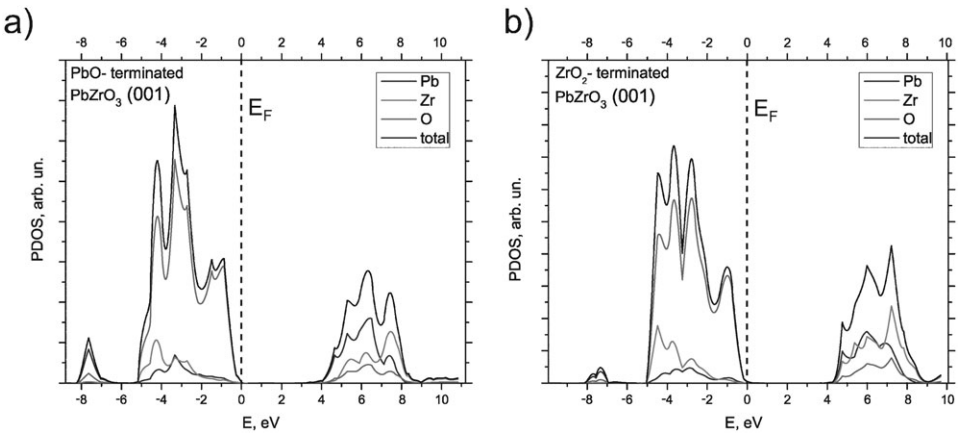

Fig. 2 Calculated total and projected density of states for PbO- (a) and ZrO_2- (b) terminated pure surfaces. E_F is taken for zero energy.

Following ref. 34 and assuming that O, Zr, and Pb do not form a condensate on the surface whereas the precipitation of their oxides does not occur, we defined a range of allowed values for Pb, Zr, and O chemical potentials as:

$$\Delta\mu_{Pb}(T,p) = \mu_{Pb}(T,p) - \gamma_{Pb}^{bulk}, \quad (3.3)$$

$$\Delta\mu_{Zr}(T,p) = \mu_{Zr}(T,p) - \gamma_{Zr}^{bulk}, \quad (3.4)$$

$$\Delta\mu_{O}(T,p) = \mu_{O}(T,p) - \frac{E_{O_2}^{total}}{2}, \quad (3.5)$$

$$\Delta G_{f_{PbZrO3}}(0,0) < \Delta\mu_{Pb}(T,p), \quad (3.6)$$

$$\Delta G_{f_{PbZrO3}}(0,0) < \Delta\mu_{Zr}(T,p), \quad (3.7)$$

$$\frac{1}{3}\Delta G_{f_{PbZrO_3}}(0,0) < \Delta\mu_{O}(T,p), \quad (3.8)$$

$$\Delta G_{f_{PbZrO3}}(0,0) < \Delta\mu_{Pb}(T,p) + 3\Delta\mu_{O}(T,p), \quad (3.9)$$

$$\Delta G_{f_{PbZrO3}}(0,0) - \Delta G_{f_{ZrO2}}(0,0) < \Delta\mu_{Pb}(T,p) + \Delta\mu_{O}(T,p) < \Delta G_{fPbO}(0,0), \quad (3.10)$$

where ΔG_f is the Gibbs free formation energy of the corresponding species. The Gibbs free formation energies calculated in the present study yield $\Delta G_{f_{PbZrO3}} = -13.96$ eV, $\Delta G_{f_{ZrO2}} = -11.22$ eV, and $\Delta G_{fPbO} = -2.38$ eV. The latter two are in perfect agreement with the experimental values of -11.37 and -2.27 eV for ZrO_2 and PbO oxides, respectively,[35] while we did not find in the literature the experimental value of $\Delta G_{f_{PbZrO3}}$. As the Gibbs free surface energy, $\Omega(T,p)$, becomes negative, surface formation becomes energetically favorable; that is, the surfaces will be formed spontaneously and the crystal will disintegrate. Therefore, the condition of the crystal existence means that $\Omega(T,p)$ is positive for all possible surfaces.

The calculated stability diagram is presented in Fig. 3a. It shows regions of oxygen and lead chemical potentials, where the surface free energies, eqn (3.1), calculated for both terminations are minimal. The precipitation of oxides is defined at limits set in eqn (3.10). The precipitation lines in Fig. 3a limit the region of the PZ stability. The areas beyond the colored regions correspond to the negative Gibbs free surface energies. The PZ bulk and surfaces are presumed to be in equilibrium with the surrounding oxygen gas atmosphere.

In contrast to DFT-PW study,[32] our thermodynamic stability diagram (Fig. 3a) definitely shows that in the range of

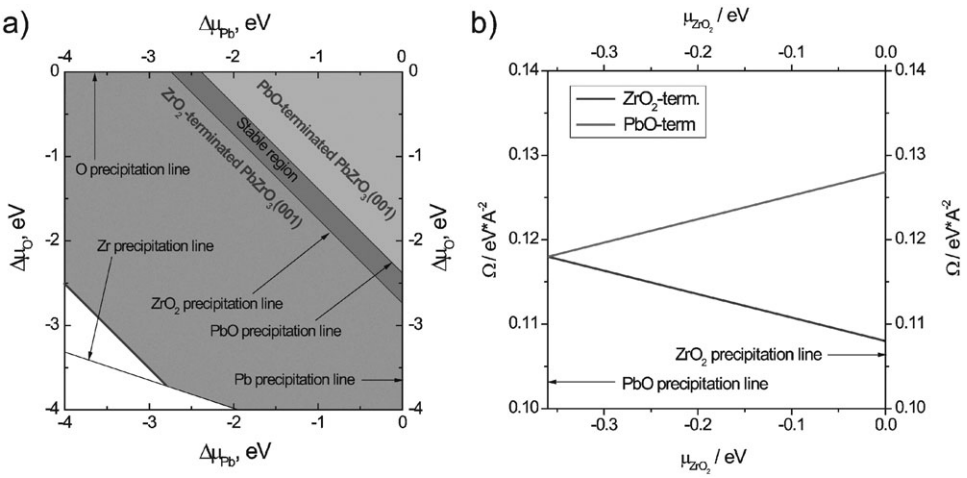

Fig. 3 Calculated thermodynamic stability diagrams, (a) with respect to precipitation of Pb, Zr, and O, (b) with respect to precipitation of PbO and ZrO_2 oxides.

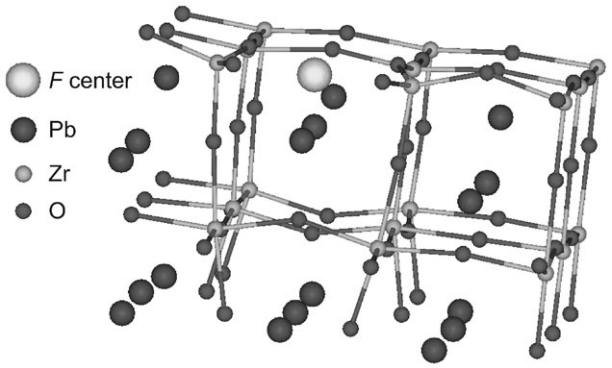

Fig. 4 Schematic view of the ZrO_2-terminated $PbZrO_3$ (001) surface structure containing the oxygen vacancy (*F* center).

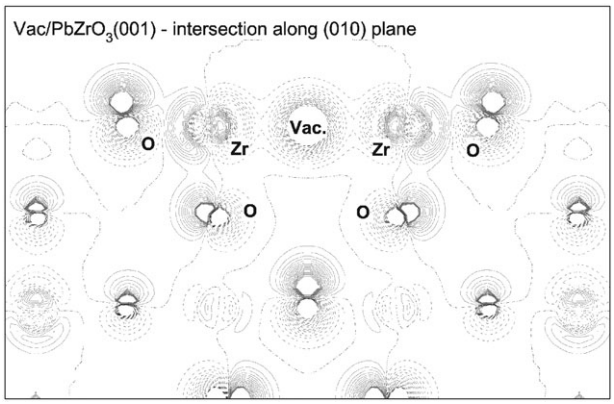

Fig. 5 Difference electron charge density map for ZrO_2-terminated $PbZrO_3$ (001) surface containing an oxygen vacancy (*F* center) in the cross section along the (010) plane. The map is the difference of the total density in the perfect $PbZrO_3$ (001) slab and the sum of electron densities of both lattices of oxygen atoms positioned in vacancy sites and a defective slab. Dashed lines mean lack of the electron density; full lines, density excess. The increment is 0.05 e a.u.$^{-3}$.

allowed chemical potentials the most stable is the ZrO_2-terminated PZ (001) surface (unshaded area between ZrO_2 and PbO precipitation line in Fig. 3a). The PbO-terminated surface becomes stable practically at the border of PbO oxide precipitation ($\sim$0.01 eV below it, see Fig. 3b). We explain disagreement with ref. 32 by a better quality of the hybrid DFT-HF functional which allowed us to improve greatly the accuracy of our analysis as compared to a standard LDA-DFT method (*e.g.* equilibrium lattice constant of bulk PZ calculated by means of LDA, a_0 = 4.09 Å,[32] is much smaller than both our a_0 calculated using the B3PW method[19] and experimental value of 4.161 Å[36]).

C Oxygen vacancy at ZrO_2-terminated surface

The positions of all atoms surrounding the *F* center at the ZrO_2 terminated surface were allowed to relax. As a result, the substantial outward relaxation is observed for both the two Zr atoms nearest to the oxygen vacancy (displacement by 0.354 Å or 8.46% of the lattice constant), as well as four nearest Pb atoms (displaced by 0.5 Å). The displacement magnitude of two Zr atoms nearest to the surface *F* center on the ZrO_2 terminated surface is comparable with that observed for Nb atoms in $KNbO_3$.[37]

The defect formation energy on the ZrO_2 terminated surface containing the O vacancy (6–7 eV) depends on the SC size (Table 3) and it is considerably smaller than that in the PZ bulk (7.25 eV). This is a driving force for the defect segregation to the surface.

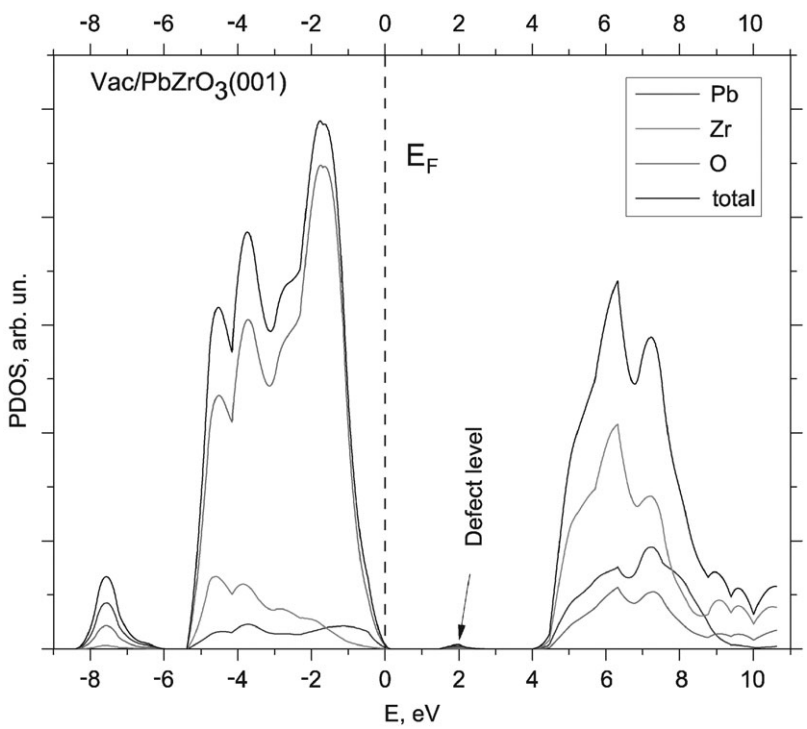

Fig. 6 Total and projected density of states of the ZrO_2-terminated (001) surface with an oxygen vacancy (*F* center). E_F is taken for zero energy.

From the difference electron charge density map (Fig. 5) and the effective charge analysis (Table 3) the conclusion could be drawn that only 0.3 e is localized inside the surface oxygen vacancy, whereas the rest electron density of the missing O^{2-} ions is delocalized over the nearest atoms. Thus, the electron localization on the surface is much weaker than in the PZ bulk (which is characterized by 0.68 e in the vacancy[19]).

Fig. 6 shows the calculated density of states for ZrO_2 terminated PZ (001) surface containing the *F* center. The DOSes look very similar to those calculated for an ideal ZrO_2-terminated surface. Defect formation results in a slightly increased band gap with respect to defectless surface structure. The surface *F* center band for the 3×3 surface supercell lies in the middle of the band gap, *i.e.* 2.58 eV below the conduction band bottom. The defect band width is very small, 0.03 eV, by a factor of five smaller than that in the bulk. This is in a sharp contrast with the calculations of the *F* center in $SrTiO_3$[15] where the *F* center is a shallow donor in both the bulk and on the surface.

IV. Conclusions

Our thermodynamic treatment predicts that ZrO_2-terminated PZ (001) surface is energetically more stable than its PbO termination. This is in contrast with the DFT-PW calculations,[32] probably due to our use of the hybrid exchange–correlation functional, which provides a much better description of the PZ(001) atomic and electronic structure.

The band gap is narrowed considerably for a pure PbO termination and slightly increased for the ZrO_2 termination. A comparison with the DFT-PW calculations shows general agreement (surfaces energy and surface rumpling) but a considerable disagreement in more refined properties such as the electronic density redistribution and band gap changes.

The *F* centers create deep defects in both PZ bulk and on the surfaces, with the energy levels located in the band gap, unlike perovskite titanates with shallow *F* centers.

(Fig. 4)

Acknowledgements

This study was supported by the Euratom-Latvia Fusion project, as well as the MRSEC Program of the National Science Foundation (DMR- 0520513) at the Materials Research Center of Northwestern University (NU), Evanston (USA). S.P. gratefully acknowledges funding from the European Social Fund (ESF). R.E. was partly supported by the German Research Council. The authors are greatly indebted to E. Heifets, E. Spohr, D. Vanderbilt, and K. M. Rabe for many helpful discussions.

References

1. S. S. Sengupta, D. Roberts, J. Li, M. C. Kim and D. A. Payne, *J. Appl. Phys.*, 1995, **78**(2), 1171–1177.
2. B. Xu, P. Moses, N. G. Pai and L. E. Cross, *Appl. Phys. Lett.*, 1998, **72**(5), 593–595.
3. B. Xu, Y. Ye and L. E. Cross, *J. Appl. Phys.*, 2000, **87**(5), 2507–2515.
4. R. Seveno, H. W. Gundel and S. Seifert, *Appl. Phys. Lett.*, 2001, **79**(25), 4204–4206.
5. H. Fujishita, Y. Ishikawa, S. Tanaka, A. Ogawaguchi and S. Katano, *J. Phys. Soc. Jpn.*, 2003, **72**(6), 1426–1435.
6. S. Teslic and T. Egami, *Acta Crystallogr., Sect. B: Struct. Sci.*, 1998, **54**, 750–765.
7. E. Sawaguchi, *Ferroelectrics*, 2002, **266**, 341–353.
8. H. Fujishita, *Ferroelectrics*, 2002, **266**, 27–40.
9. M. D. Johannes and D. J. Singh, *Phys. Rev. B: Condens. Matter Mater. Phys.*, 2005, **71**, 2121011–2121014.
10. K. Leung and A. F. Wright, *Ferroelectrics*, 2002, **281**, 171–186.
11. J. A. Rodriguez, A. Etxeberria, L. González and A. Maiti, *J. Chem. Phys.*, 2002, **117**(6), 2699–2709.
12. S. S. N. Bharadwaja and S. B. Krupanidhi, *J. Appl. Phys.*, 2001, **89**(8), 4541–4547.
13. J. Zhai and H. Chen, *Appl. Phys. Lett.*, 2003, **82**(16), 2673–2675.
14. R. Bittner, K. Humer, H. W. Weber, K. Kundzins, A. Sternberg, D. A. Lesnyh, D. V. Kulikov and Y. V. Trushin, *Integr. Ferroelectr.*, 2005, **72**, 47–51.
15. Y. F. Zhukovskii, E. A. Kotomin, R. A. Evarestov and D. E. Ellis, *Int. J. Quantum Chem.*, 2007, **107**, 2956–2985.
16. S. Piskunov, E. Heifets, R. I. Eglitis and G. Borstel, *Comput. Mat. Sci.*, 2004, **29**(2), 165–178.
17. R. I. Eglitis, S. Piskunov, E. Heifets, E. A. Kotomin and G. Borstel, *Ceram. Int.*, 2004, **30**, 1989–1992.
18. S. Piskunov, E. A. Kotomin, E. Heifets, J. Maier, R. I. Eglitis and G. Borstel, *Surf. Sci.*, 2005, **575**, 75–88.
19. S. Piskunov, A. Gopeyenko, E. A. Kotomin, Y. F. Zhukovskii and D. E. Ellis, *Comput. Mat. Sci.*, 2007, **41**, 195–201.
20. Crystal06 User's Manual. R. Dovesi, V. R. Saunders, C. Roetti, R. Orlando, C. M. Zicovich-Wilson, F. Pascale, B. Civalleri, K. Doll, N. M. Harrison, I. J. Bush, Ph. D'Arco and M. Llunell, University of Torino, Torino, 2006.
21. A. D. Becke, *J. Chem. Phys.*, 1993, **98**(7), 5648–5652.
22. J. P. Perdew and Y. Wang, *Phys. Rev. B: Condens. Matter Mater. Phys.*, 1986, **33**(12), 8800–8802.
23. J. P. Perdew and W. Yue, *Phys. Rev. B: Condens. Matter Mater. Phys.*, 1989, **40**(5), 3399.
24. J. P. Perdew and Y. Wang, *Phys. Rev. B: Condens. Matter Mater. Phys.*, 1992, **45**(23), 13244–13249.
25. P. J. Hay and W. R. Wadt, *J. Chem. Phys.*, 1984, **82**(1), 270–283.
26. P. J. Hay and W. R. Wadt, *J. Chem. Phys.*, 1984, **82**(1), 284–298.
27. H. J. Monkhorst and J. D. Pack, *Phys. Rev. B: Solid State*, 1976, **13**(12), 5188–5192.
28. J. Padilla and D. Vanderbilt, *Surf. Sci.*, 1998, **418**, 64–70.
29. C. Cheng, K. Kunc and M. H. Lee, *Phys. Rev. B: Condens. Matter Mater. Phys.*, 2000, **62**(15), 10409–10418.
30. H. B. Schlegel, *J. Comput. Chem.*, 1982, **3**, 214–218.
31. B. Civalleri, P. D'Arco, R. Orlando, V. R. Saunders and R. Dovesi, *Chem. Phys. Lett.*, 2001, **348**(ER1-2), 131–138.
32. Y. X. Wang, *Phys. Status Solidi B*, 2007, **244**(2), 602–609.
33. E. Heifets, R. I. Eglitis, E. A. Kotomin, J. Maier and G. Borstel, *Phys. Rev. B: Condens. Matter Mater. Phys.*, 2001, **64**, 235417.
34. E. Heifets, S. Piskunov, E. A. Kotomin, Y. F. Zhukovskii and D. E. Ellis, *Phys. Rev. B: Condens. Matter Mater. Phys.*, 2007, **75**(11), 115417.
35. I. Barin and G. Platzki, *Thermochemical data of pure substances*, VCH, Weinheim, New York, 3rd edn, 1995.
36. S. Aoyagi, Y. Kuroiwa, A. Sawada, H. Tanaka, J. Harada, E. Nishibori, M. Takata and M. Sakata, *J. Phys. Soc. Jpn.*, 2002, **71**(10), 2353–2356.
37. R. I. Eglitis, N. E. Christensen, E. A. Kotomin, A. V. Postnikov and G. Borstel, *Phys. Rev. B: Condens. Matter Mater. Phys.*, 1997, **56**(14), 8599–8604.